# Making corrections to your proof

Please follow these instructions to mark changes or add notes to your proof. Ensure that you have downloaded the most recent version of Acrobat Reader from **https://get.adobe.com** so you have access to the widest range of annotation tools.

The tools you need to use are contained in **Annotations** in the **Comment** toolbar. You can also right-click on the text for several options. The most useful tools have been highlighted here. If you cannot make the desired change with the tools, please insert a sticky note describing the correction.

Please ensure all changes are visible via the 'Comments List' in the annotated PDF so that your corrections are not missed.
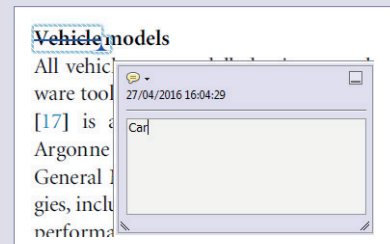
Attach file
Highlight text
Insert sticky note
Insert text
Replace text
Strikethrough text
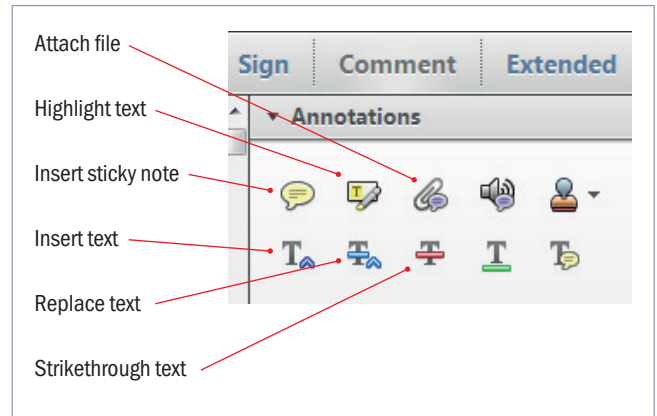
Do not attempt to directly edit the PDF file as changes will not be visible.
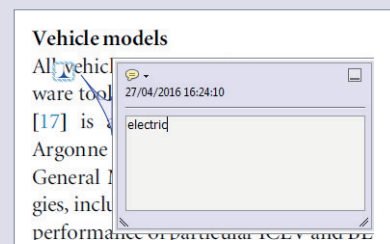
Replacing text
To replace text, highlight what you want to change then press the replace text icon, or right-click and press 'Add Note to Replace Text', then insert your text in the pop up box. Highlight the text and right click to style in bold, italic, superscript or subscript.

Vehicle models
All vehic
ware tool
[17] is a
Argonne
General l
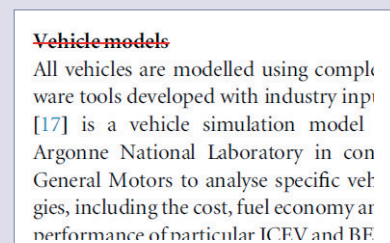gies, incl
performa
27/04/2016 16:04:29
Car

Inserting text
Place your cursor where you want to insert text, then press the insert text icon, or right-click and press 'Insert Text at Cursor', then insert your text in the pop up box. Highlight the text and right click to style in bold, italic, superscript or subscript.
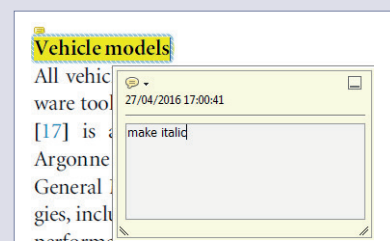
Vehicle models
All vehicl
ware tool
[17] is a
Argonne
General l
gies, inclu
performance of particular ICEV and BE
27/04/2016 16:24:10
electric

Deleting text
To delete text, highlight what you want to remove then press the strikethrough icon, or right-click and press 'Strikethrough Text'.

Vehicle models
All vehicles are modelled using comple
ware tools developed with industry inpr
[17] is a vehicle simulation model
Argonne National Laboratory in con
General Motors to analyse specific vel
gies, including the cost, fuel economy an
performance of particular ICEV and BE

Highlighting text
To highlight text, with the cursor highlight the selected text then press the highlight text icon, or right-click and press 'Highlight text'. If you double click on this highlighted text you can add a comment.

Vehicle models
All vehic
ware tool
[17] is a
Argonne
General l
gies, inclu
performa
27/04/2016 17:00:41
make italic

QUERIES

Page 1
AQ1
Please check that the names of all authors as displayed in the proof are correct, and that all authors are linked correctly to the appropriate affiliations. Please also confirm that the correct corresponding author has been indicated.
AQ2
Please specify the corresponding author and provide his/her email address.
AQ3
Please be aware that the colour figures in this article will only appear in colour in the online version. If you require colour in the printed journal and have not previously arranged it, please contact the Production Editor now.
Page 2
AQ4
Please check and approve the edits made to this sentence, or provide an alternative that conveys the intended meaning.
AQ5
We have changed 'few' to 'some' here. Please check and approve.
Page 3
AQ6
We have changed Map-2 to MAP2, as on page 13. Please check and approve.
AQ7
Please check the inclusion of 'Life Science' for its appropriateness.
Page 7
AQ8
We have changed 'outlayers' to 'outliers'. Please check and approve.
Page 10
AQ9
Please check that the funding information below is correct for inclusion in the article metadata. Fondazione Umberto Veronesi; European Union (FP7-PEOPLE-2012-ITN): NANOMICROWAVE project number 317116.
AQ10
If an explicit acknowledgment of funding is required, please ensure that it is indicated in your article. If you already have an Acknowledgments section, please check that the information there is complete and correct.
AQ11
Please check the details for any journal references that do not have a link as they may contain some incorrect information. If any journal references do not have a link, please update with correct details and supply a Crossref DOI if available.
AQ12
Reference [1] is listed in the reference list but not cited in the text. Please cite in the text, else delete from the list.
Page 11
AQ13
Please provide the page/article number details for references [45, 47].

Acoustic stimulation can induce a selective neural network response mediated by piezoelectric nanoparticles

Camilo Rojas[1], **Mariateresa Tedesco**[1], **Paolo Massobrio**[1], **Attilio Marino**[2], **Gianni Ciofani**[2,3], **Sergio Martinoia**[1,4] **and Roberto Raiteri**[1,4]

[1] Department of Informatics, Bioengineering, Robotics, and System Engineering, University of Genova, via Opera pia 13, 16145 Genova, Italy
[2] Smart Bio-Interfaces, Istituto Italiano di Tecnologia, Viale Rinaldo Piaggio 34, 56025 Pontedera, Italy
[3] Department of Mechanical and Aerospace Engineering, Politecnico di Torino, Corso Duca degli Abruzzi 24, 10129 Torino, Italy
[4] National Council of Research (CNR)—IBF Institute, via de Marini 6, 16149 Genova, Italy

AQ2 E-mail: xxxx

Abstract

Objective. We aim to develop a novel non-invasive or minimally invasive method for neural stimulation to be applied in the study and treatment of brain (dys)functions and neurological disorders. *Approach*. We investigate the electrophysiological response of *in vitro* neuronal networks when subjected to low-intensity pulsed acoustic stimulation, mediated by piezoelectric nanoparticles adsorbed on the neuronal membrane. *Main results*. We show that the presence of piezoelectric barium titanate nanoparticles induces, in a reproducible way, an increase in network activity when excited by stationary ultrasound waves in the MHz regime. Such a response can be fully recovered when switching the ultrasound pulse off, depending on the generated pressure field amplitude, whilst it is insensitive to the duration of the ultrasound pulse in the range 0.5 s–1.5 s. We demonstrate that the presence of piezoelectric nanoparticles is necessary, and when applying the same acoustic stimulation to neuronal cultures without nanoparticles or with non-piezoelectric nanoparticles with the same size distribution, no network response is observed. *Significance*. We believe that our results open up an extremely interesting approach, when coupled with suitable functionalization strategies of the nanoparticles in order to address specific neurons and/or brain areas and applied *in vivo*, enabling remote, non-invasive and highly selective modulation of the activity of neuronal subpopulations of the central nervous system of mammalians.

Keywords: ultrasound neuromodulation, barium titanate nanoparticles, microelectrode array

S Supplementary material for this article is available online

(Some figures may appear in colour only in the online journal)

Introduction

Neural stimulation and modulation techniques are recognized as key enabling tools in neuroscience, allowing for the treatment of neurological diseases and the investigation of brain (dys)functions [2]. Among them, deep brain stimulation (DBS) is a well-recognized approach, commonly used to provide AC electrical stimulation using chronically implanted electrodes, generally targeting areas such as the thalamus, a portion of the *globus pallidus*, or the sub-thalamic nucleus. DBS has shown the capability of recovering symptoms in patients with motor disorders such as Parkinson's disease [3], and with other psychiatric and neurological disorders such as obsessive-compulsive disorders, depression,

1

epilepsy, schizophrenia, pain, and Alzheimer's disease [4]. Nevertheless, such a technique requires rather invasive surgery for the placement of the electrodes close to the targeted area, which increases the risk of infection [5], and it suffers from poor long-term biocompatibility [6].

New generations of less invasive neural stimulation/modulation techniques have been proposed, including transcranial magnetic stimulation (TMS), transcranial direct current stimulation (tDCS), and *vagu*s nerve stimulation (VNS) [7]. Their common goal is the generation of electrical fields localized in different brain regions, with a spatial resolution on the order of a few centimeters [8, 9]. As a consequence, this poor resolution results in non-specific stimulation of the brain regions surrounding the target area [10].

Ultrasound (US) has been used in an extensive range of medical applications, including brain stimulation, since it potentially combines non-invasiveness with high spatial selectivity. Naor and colleagues recently thoroughly reviewed the achievements and challenges of ultrasonic neuromodulation [11]. By carefully selecting the frequency and intensity, and by employing suitable transducers (e.g. multi-element, phased array ultrasound systems), US can be virtually focused to any region of interest in the human brain, using either pulsed or continuous waveforms, with a spatial resolution down to the millimeter scale [12, 13]. A solid mechanistic understanding of the biophysical effects produced by US on neural tissue is still to come; nevertheless such effects can be roughly divided into thermal and non-thermal. Thermal effects are the consequence of high acoustic intensities [14], which can cause 'disruptive' effects such as cavitation. A temperature increase can cause denaturation of the proteins involved in neurotransmission, thus determining a decrease in the synaptic transmission, and consequently, neuronal activity suppression. Non-thermal effects are related to lower intensity waves [15] providing a mechanical stimulus (referred to as 'radiation pressure'), which might change the viscoelasticity of the cell membrane, activate the mechano-sensitive transmembrane proteins, or induce *intramembrane cavitation* [16]. There is some experimental evidence that US stimulation is capable of modulating ion channel currents [17], activating action potentials and synaptic transmission *in vitro* [15, 18], or, for example, stimulating the motor cortex and the mouse hippocampus *in vivo* [19]. Importantly, most of the studies substantially agree that it is possible to provide US stimulation capable of manipulating neural activity without inducing tissue damage [16, 20, 21].

Recently, novel nanomaterials have been implemented in neural stimulation techniques to improve performance in terms of efficiency and selectivity [22, 23]. The working principle is based on a primary stimulus from an external source (light, magnetic field, or acoustic wave) which is converted by the nanomaterial into a secondary stimulus focused in the region of interest. As an example, light is used as a first stimulus that is converted by quantum dots [24, 25] and gold nanoshells [26] or nanorods [27] into an electric field and heat, respectively. With a similar approach, by applying electromagnetic fields as a primary stimulus and by exploiting magneto-electric [28] transduction or superparamagnetic [29] nanoparticles as localized transducers, it is possible to convert the first stimulus in a localized electrical field [30], temperature increase [30, 31] or mechanical force [32, 33].

Piezoelectric nanomaterials have been proposed as acoustic-electric transducers to convert remotely generated US into locally generated electric fields [34, 35]. Some of us have recently shown that piezoelectric barium titanate nanoparticles (BTNPs) organized in a tetragonal lattice structure induce a Ca^{2+} influx in a 'neuron-like' cell culture (SH-SY5Y cell line) as a response to ultrasound [36]. Such an effect has been interpreted in terms of transduction of the primary mechanical stimulus (in this case US at 1 MHz generated with a power of 1 W cm^{-2}) into a localized (close to the cell membrane) electrical field by BTNPs. In this work, we further investigate this approach by using primary cultures of cortical and hippocampal neurons coupled with micro-electrode arrays (MEAs), capable of performing electrophysiological recording to investigate the presence of direct evidence for neuronal activation due to the stimulation of US, mediated by the presence of piezoelectric BTNPs.

Methods

Preparation and characterization of the BTNPs

In this work we used piezoelectric non-centrosymmetric BTNPs, characterized by a tetragonal crystal phase (1144DY, from Nanostructured and Amorphous Materials, Inc. Houston, TX). The nanomaterial composition and its level of purity were provided by the supplier: BaO/TiO$_2$ 0.999–1.001; average particle size (APS): 300 nm; specific surface area (SSA): 3.5–3.7 m^2 g^{-1}; purity 99.9%.

As previously reported [36], the BTNPs were stabilized in phosphate buffered saline (PBS) solution by noncovalent wrapping with gum arabic (G9752, from Sigma-Aldrich) and dispersed in water by sonication. The nanoparticle dispersion (10 mg ml^{-1}) was further sonicated for 30 min using a Bransonic sonicator 2501 to obtain a homogeneous suspension, right before subsequent dilution (1:200) in cell culture medium at the final concentration of 50 μg ml^{-1} for biological experiments.

Analogous BTNPs, characterized by a centrosymmetric cubic crystal structure (1143DY, from Nanostructured and Amorphous Materials) were adopted for the control experiments, following the same preparation procedure and dilution.

The imaging of nanoparticles was carried out with a scanning electron microscope (SEM, Helios NanoLab 600i FIB/SEM, FEI). Specifically, a stable water dispersion of 50 μg ml^{-1} of cubic or tetragonal BTNPs wrapped with gum arabic was deposited on a silica substrate. The samples were dried for 4 h and subsequently gold-sputtered.

The dispersions (50 μg ml^{-1} cubic or tetragonal BTNPs) were finally analyzed in terms of Z-potential and hydrodynamic radius with a Nano Z-Sizer 90 (Malvern Instruments).

Neuronal network preparation

To obtain stable and long-lasting neuronal network activity, the MEA chips were sterilized and treated with adhesion molecules—laminin and poly-D-lysine at the same concentration of 0.05 mg ml^{-1} (both from Sigma-Aldrich)—to favor neuronal adhesion and growth. Rats were sacrificed and 18 d embryos (E18) were removed immediately by cesarean section. All procedures were carried out to reduce the number of animals and to minimize their suffering. The experimental protocol was approved by the European Animal Care Legislation (2010/63/EU), by the Italian Ministry of Health in accordance with the D.L. 116/1992, and by the guidelines of the University of Genova (Prot. N. 24982, October 2013).

Cell culture. The hippocampus and cortex were removed from the rat embryo, their tissue was first enzymatically dissociated in 0.125% of Trypsin/Hank's solution containing 0.05% DNAse (Sigma Aldrich) for 18–20 min at 37 °C, and then mechanically dissociated with a fire-polished Pasteur pipette. Cells were plated on the MEAs at a density of about 1600 cells mm^{-2} in a solution containing Neurobasal™ Medium with 1% glutamax, 2% B-27 supplemented and 1% penicillin–streptomycin (all from Invitrogen Life Technologies). The MEAs were then incubated in a humidified 5% CO_2 atmosphere at 37 °C and a half-volume medium was replaced every week. More details about the procedure that followed to prepare the neuronal networks on the MEA can be found in [37]. The experiments were performed after at least 21 d *in vitro* (DIV).

BTNP treatment. The evening before the experiment, a half volume (750 μl) of the medium was directly withdrawn from the culture chip. Then, 75 μl of the BTNP suspension, which had been sonicated immediately before again for 10 min, was added to the culture. Finally, the chip was filled with the missing 750 μl of medium and incubated overnight at 37 °C, 5% CO_2 at 95% humidity.

Immunostaining and confocal imaging. Immediately after some randomly selected experiments, cultures were fixed using 4% paraformaldehyde in PBS for 20 min at room temperature. Repeated washing was done with PBS to remove the fixative as a post-fixation step, followed by a permeabilization step with a Triton X-100 0.2% (8 min); finally, the cultures were exposed to a blocking buffer solution (PBS with 2% bovine serum albumin (BSA), 0.5% fetal bovine serum (FBS)). Antibodies raised against the specific markers NeuN and MAP2 were used and visualized by the Alexa Fluor 549-Gam (goat anti-mouse IgG) and Alexa Fluor 488-Gar (goat anti-rabbit IgG) secondary antibodies (Thermo Fisher Scientific, Waltham, MA) in order to locate the neuronal soma and dendrites, respectively. Fluorescence imaging of the immunostained samples was performed with a confocal laser scanning microscope (C2s, Nikon). Specifically, 488 and 561 nm lasers were used for the excitation of Alexa Fluor 488 Gar Alexa Fluor Gam and 549, and the emission lights were collected at 500–550 and 570–630 nm, respectively. BTNPs were

detected through confocal fluorescence imaging by using far red laser excitation (excitation at 642 nm and collection from 650 to 1000 nm), as previously indicated [36].

Inhibitory cocktail. In order to inhibit synaptic communication we used a cocktail of synaptic receptor antagonists constituted by (-)-bicuculline methiodide (BIC) 20 μM, DL-2-amino-5-phosphonopentanoic (APV) 50 μM and 6-cyano-7-nitroquinoxaline-2,3-dione disodium (CNQX) 30 μM (Sigma-Aldrich, Life Science).

Experimental set-up

Ultrasound stimulation

MEA chips (Multi Channel Systems MCS GmbH, Reutlingen, Germany) with glass rings were filled with a culture medium and covered with Parafilm M®. A commercial US source (model SonoPore KTAC-4000 by Nepa Gene Co., Ltd, Japan) equipped with a disc-shaped piezoelectric transducer (model KP-S20, diameter size: 20 mm, working frequency: 1 MHz) was employed. We added some acoustically transparent gel (Pharmaceutical Innovations Inc., Newark, NJ) to couple the ultrasound probe with the Parafilm cap. The US transducer was placed parallel to the MEA surface at an 8 mm distance from the neuronal culture. The generated pressure field was characterized by directly measuring its intensity using a dummy MEA chip with a hole drilled in the microelectrode array area to allow the insertion of a calibrated miniaturized hydrophone (TC4038, Teledyne Reson, Denmark). After filling the chamber with the culture medium, closing its top with Parafilm, and placing the US transducer, we measured the pressure intensity as a function of the vertical position of the hydrophone and the power of the US generator. The dummy chamber was also equipped with a miniaturized thermocouple in order to measure any temperature increase due to US.

MEA set-up

The electrophysiological activity from the cortical and hippocampal neuronal networks was recorded by means of a commercial MEA recording system (MEA 2100, Multi Channel Systems MCS GmbH, Reutlingen, Germany). In this work, we used MEA chips made up of 60 TiN/SiN microelectrodes (30 μm diameter and 200 μm pitch distance) arranged in an 8 × 8 square grid (the four electrodes in the corners are not present). One of the electrodes in the array is used as a pseudo-reference electrode for extracellular field potential recording from the remaining 59. The raw data was acquired with the proprietary software (MC_Rack, Multi Channel Systems MCS GmbH, Reutlingen, Germany) at a 10 kHz sampling frequency. This software also recorded a custom-generated digital signal defining the pulse train by triggering on and off US generation. During off-line analysis, a Matlab (The MathWorks Inc., Natick, MA) script used the recorded digital signal to allow the synchronization of the signals from the electrodes with the generation of US and to remove single

glitches in the electrode recordings due to the switching on and off of the US generator.

Experimental protocol

The US stimulation protocol consists of a train of US pulses with 2 s periodicity and a variable duty cycle. For all the reported experiments, if not differently specified, a duty cycle of 50% was used for a total duration of 180 s (90 periods). The electrophysiological activity of the neuronal network under test is recorded from the electrodes of the MEA device before, during and after US stimulation (figure 1(g)). To further check the responsiveness of the neuronal network to external stimulation, we delivered low-frequency electrical stimulation through a randomly selected microelectrode in the array [38] at the end of each experimental session (supporting methods and figure S4 (stacks.iop.org/JNE/00/0000/mmedia)).

Data analysis

Data analysis was performed using SPYCODE software [39] and additional *ad hoc* scripts developed in Matlab.

Spike detection. Spikes were detected using the precise timing spike detection (PTSD) algorithm [40]. Spike trains are computed by setting three parameters: a differential threshold (set independently for each channel) set to seven times the standard deviation of the biological noise of the signal, the peak lifetime period (set to 4 ms) and the refractory period (set to 2 ms). The data has not been spike sorted, because during bursting activity the fast sequence of spikes with different and overlapping shapes makes sorting difficult and unreliable [41].

Mean firing rate (MFR). The MFR is the firing rate relative to each active electrode (i.e. a firing rate greater than 0.2 spikes s^{-1}) averaged among all the active electrodes of the MEA.

Post-stimulus time histogram (PSTH). The PSTH was evaluated considering a temporal window of 2 s after the delivery of each stimulus. Such a 2 s temporal window is divided into bins of 50 ms, and then the number of spikes that has fallen into each bin is counted. Finally, the histograms of each channel were normalized over the number of stimuli (90) and the bin size.

Statistical analysis. Since the data does not follow a normal distribution, the Wilcoxon rank-sum test was used for the statistical analysis to check significant changes between the two distributions. The data was processed for statistical analysis and plotted as a mean value ± standard error.

Results

We tested the proposed acoustic stimulation technique on primary cultures of cortical and hippocampal neurons from rat embryos plated onto MEAs (figure 1(a)). After 21 d *in vitro* (DIV), mature neuronal networks were incubated with BTNPs overnight.

The scanning electron microscopy images of BTNPs show quite a homogeneous round-like shape (figure S1). The hydrodynamic radius size of the cubic crystal BTNPs (116.8 ± 46.5 nm; polydispersity index of 0.165), showing piezoelectric behavior, were slightly smaller with respect to the tetragonal ones (156.5 ± 42.5 nm; polydispersity index of 0.254), which do not show piezoelectric behavior. The Z-potential of the BTNPs characterized by cubic (−38.8 ± 5.8 mV) and tetragonal (−40.7 ± 4.9 mV) phases were comparable, thus making them comparable in terms of the nanoparticle–cell interface, despite the difference in size.

Microscopy images of the neuronal cultures taken after the experiments allowed us to verify the presence and distribution of the BTNPs (figures 1(b) and (c), and supporting figures S2 and S3). We also observed that the nanoparticles were associated with the selectively stained neural plasma membrane with no significant internalization, even after 24 h incubation time (figure S3 and video S1).

During the experimental session, we applied US stimulation by placing a planar disc transducer on top of the MEA chamber, filled with a culture medium and sealed with a thin plastic film (Parafilm®) (figures 1(d) and (e)). The generated stationary pressure field was calibrated using a miniaturized hydrophone placed on the bottom of a dummy MEA chamber as a function of the nominal signal power generated by the US source (figure 1(f)), showing good linearity.

Each electrode of the MEA records the spontaneous electrophysiological activity of the neurons (i.e. extracellular action potentials). Figure 1(h) shows an example of a typical signal from one electrode where spiking activity (originating from different neurons close to the electrode) occurs in a short period of time, thus generating typical bursting behavior (i.e. sequences of densely packed spikes).

When neuronal networks incubated with piezoelectric BTNPs were exposed to US, we observed an evident increase in recorded activity with respect to spontaneous activity before and after the stimulation. As an example of such a modulated response, figure 2 shows a representative Raster plot of the detected spikes recorded from the cortical culture at DIV 21. It can be directly observed that the spiking activity, which is indeed present before and after stimulation (i.e. spontaneous activity), increases during the stimulation (figure 2(a)). Qualitative analysis of the Raster plot at a higher time resolution (red boxes in figure 2(b)) shows an evident increase of neural activity in the time intervals during which the US generation is switched on (US$_{ON}$). To quantify the network activity, we calculated the mean network firing rate (MFR) as the average number of spikes per second detected by all the recording and active electrodes (i.e. electrodes measuring at least 0.2 spike s^{-1}) over the total duration of the US pulses (90 s for a pulse train with a 2 s period, 50% duty cycle and 180 s total duration), the intervals between US pulses, and the same time interval right before the pulse train (respectively, US$_{ON}$, US$_{OFF}$ and baseline in figure 2(c)). We also verified that the response of neurons to US in the presence of piezoelectric BTNPs can be fully recovered and reproduced by repeating the stimulation on the same network three times, with 5 min recovery
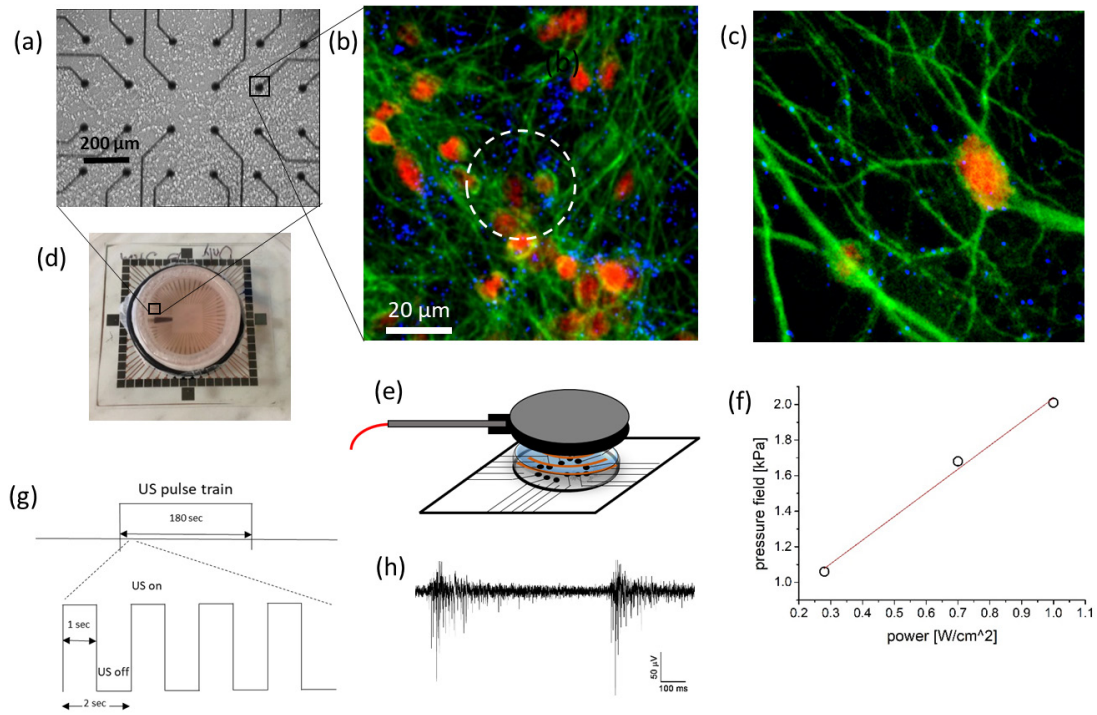
Figure 1. The experimental set-up for US stimulation. (a) A bright-field microscopy image of neurons cultured on an array of TiN microelectrodes (30 μm in diameter, visible as dark discs). (b) The confocal image of a region around a single microelectrode (dashed circle) with neurons treated with BTNPs. Neuron soma (NeuN, orange), neurites (MAP2, green) are identified by immunostaining, as well as the autofluorescence signal of the BTNPs (blue). (c) The zoom of an area around a single neuron. (d) An image of the MEA chip filled with culture medium and encapsulated in Parafilm M®. (e) A schematic view of the US transducer positioned on top of the sealed MEA chamber and generating US. (f) The measured pressure field amplitude as a function of the nominal power of the generated US (red line: linear regression). (g) The acoustic stimulation protocol: spontaneous activity is recorded for 5 min before, during and after US stimulation, which is applied as a train of pulses with a duration of 1 s and 2 s. (h) An example of the raw signal recorded from one microelectrode over 1.5 s. Action potentials can be identified as 'spikes'.
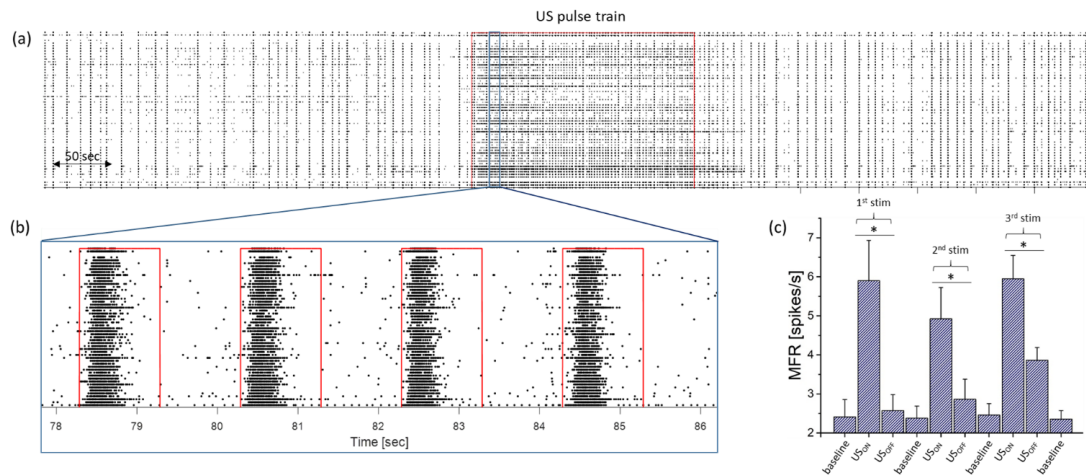

Figure 2. The effect of US stimulation on neuronal network activity mediated by BTNPs. (a) A representative Raster plot of the activity of a neuronal network incubated with piezoelectric BTNPs before, during and after the stimulation interval with the US pulse train (red box). (b) A zoomed Raster plot where 1 s intervals corresponding to the US pulses can be identified (red boxes). (c) A plot of the mean network firing rate (MFR) during repeated stimulations of the same neuronal culture. Three subsequent US stimulations were performed, with resting intervals in between. MFR values were calculated over 90 s intervals before ('baseline') and during the stimulation phase. 'US on' and 'US off' represent the intervals (50% of 2 s * 90 periods = 90 s) during which the US source was switched on and off in the stimulation phase, respectively (*$P < 0.05$, Wilcoxon test).

intervals in between. We observed similar, statistically significant (Wilcoxon signed rank sum, $p < 0.05$) increases of the MFR for each US_{ON} interval, with an almost complete recovery to the original baseline level as soon as the US source was switched off in the pulse train (i.e. US_{OFF} interval), as reported in figure 2(c).

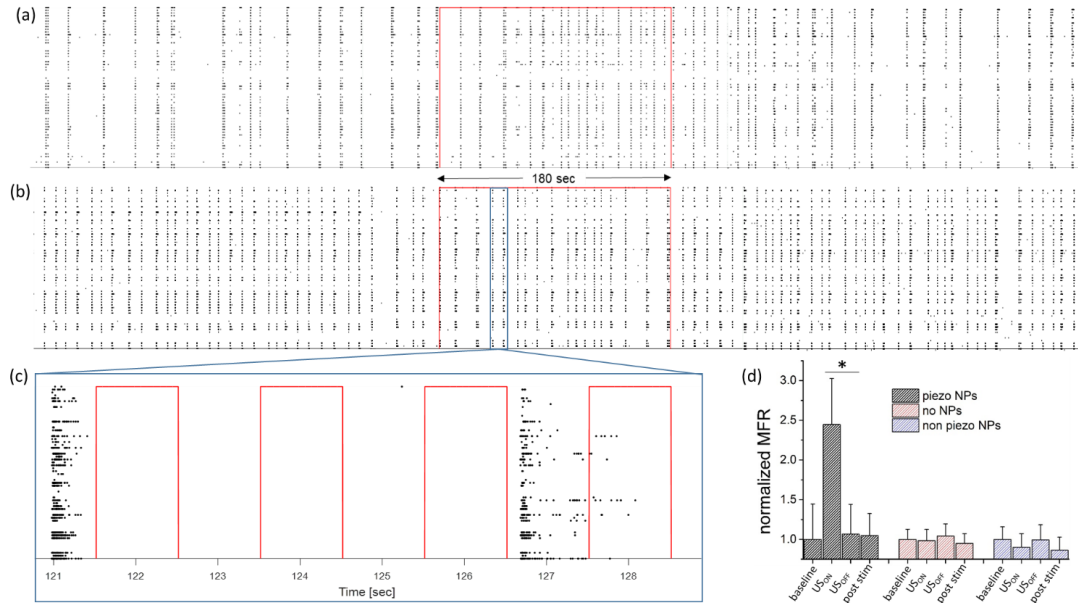Control experiments were performed with neuronal networks without BTNPs, or incubated with non-piezoelectric

Figure 3. Representative Raster plots before, during and after US stimulation of a neuronal network without BTNPs (a) and incubated with non-piezoelectric BTNPs (b). (c) The zoomed interval during US stimulation (red frames indicate the intervals during which the US source was switched on). (d) Mean network firing rates (MFR) calculated for the three experiments reported in figure 2(a) (black columns) and in panels (a) and (b) (red and blue columns, respectively). In order to compare the MFR values, they were normalized to the MFR value of the corresponding baseline for each experiment ($^*P < 0.05$, Wilcoxon signed rank test).
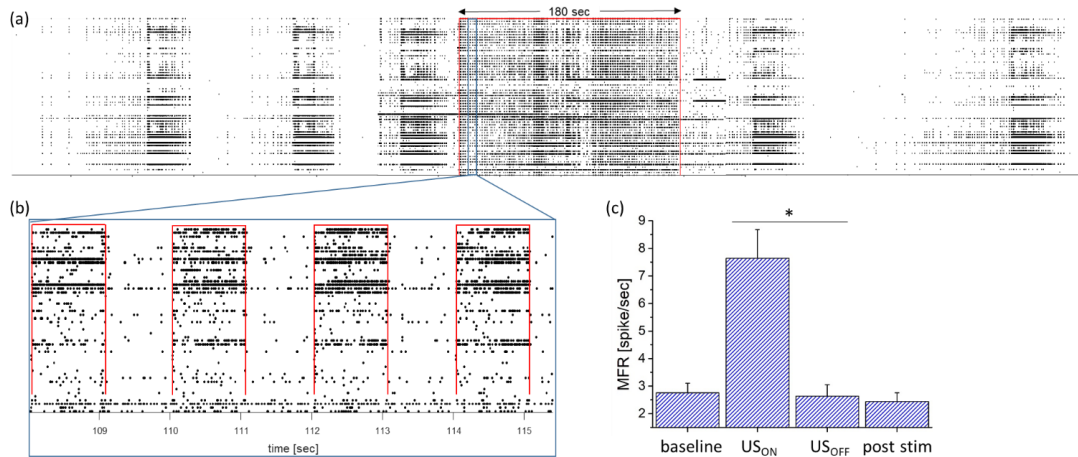

Figure 4. A representative experiment of the US stimulation of a hippocampal neuronal network incubated with piezoelectric BTNPs. (a) A Raster plot before, during and after US stimulation. (b) A zoomed interval during US stimulation (red frames indicate the intervals during which the US source was switched on). (c) A plot of the MFR calculated for 90 s intervals before ('baseline'), during ('US on', and 'US off') and after ('post stim') the stimulation phase ($^*P < 0.05$, Wilcoxon signed rank test).

BTNPs, which are characterized by a cubic crystal structure. In neither case did we observe a significant response to US, although the same cultures at the end of the experiments responded to the electrical stimulation as expected (see supporting figure S4(b)). Figure 3 reports two examples of the recorded Raster plots from cortical networks without nanoparticles and with non-piezoelectric BTNPs (figures 3(a) and (b), respectively). When zooming the time scale during the stimulation phase, it becomes clear that the firing activity is not affected by the US pulses (figure 3(c)). We computed the MFR for time intervals before, during and after US stimulation. In general, the spontaneous activity of neuronal networks coming from different or even the same preparation can vary a lot in terms of firing rate and the presence of stereotyped

bursting activity [42]. In order to compare the responses from different cultures, for each experiment we normalized the MFR to the corresponding value calculated before the stimulation phase (baseline) (figure 3(d)).

We applied the same protocol to hippocampal cultures incubated with piezoelectric BTNPs (the same procedure as for cortical cultures). Figure 4 reports a representative example of such experiments. In this case, the spontaneous activity shows more complex and synchronized firing patterns than those observed in the previous examples. Nevertheless, it is again possible to qualitatively detect, from the Raster plot, a clear increase of the firing rate that is correlated to the US pulses (figures 4(a) and (b)). The quantification of the MFR value before, during (US$_{ON}$ and US$_{OFF}$ intervals) and
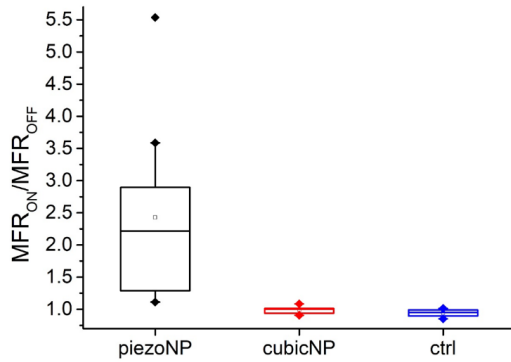
Figure 5. A Tukey boxplot (including outliers) summarizing the US stimulation experiments performed with piezoelectric BTNPs ($n = 10$) and control experiments ($n = 5$ with non-piezoelectric NPs, $n = 4$ without NPs). In order to compare different experiments performed with neuronal preparations from the cortex or the hippocampus, the ratio between the mean network firing rate during 'US on' (MRF$_{ON}$) and 'US off' (MRF$_{OFF}$) intervals for each experiment was calculated and reported.

Figure 6. The dependence of the neural network response to the pressure field intensity generated by the US. The ratio between the mean network firing rate during the 'US on' and 'US off' intervals (MRF$_{ON}$ and MRF$_{OFF}$ respectively) is plotted as a function of the pressure field intensity; red line: linear regression ($r^2 = 0.99475$).

after the stimulation phase, shows the statistically significant ($p < 0.05$, Wilcoxon signed rank test) effect of US stimulation on network activity, which is completely recovered after the stimulation phase.

To further investigate the reproducibility of the observed responses to US, we repeated the same type of experiment with different neuronal preparations from five different animals, using either neurons from the cortex or the hippocampus, for a total of $n = 22$ MEAs. Thirteen cultures were treated with piezoelectric BTNPs, while nine cultures were considered as controls, four without BTNPs and five with non-piezoelectric BTNPs. We obtained consistent results despite the high variability in spontaneous activity. At the end of each experimental session, a final phase of electrical stimulation, by applying uncorrelated voltage pulses for 3 min from at least two electrodes, was performed (supporting methods and figure S4). The rationale was to verify the responsiveness of the network to electrical pulse trains, as is usually done for these experimental preparations, and to correlate it with the responsiveness to US stimulation. All cultures incubated with piezoelectric BTNPs which showed a response to electrical stimulation (ten out of the thirteen available samples) were also sensitive to US stimulation. The remaining $n = 2$ cases were insensitive to both electrical and US stimulation. None of the $n = 9$ control cultures showed any response to US, while they all responded to electrical stimulation. Figure 5 reports a summary of all the performed experiments, where we observed a response to electrical stimulation.

In order to allow a quantitative and compact comparison of the different experiments, characterized by a large variability in spontaneous activity, for each experiment we calculated the ratio between the MFR during the US$_{ON}$ interval (MFR$_{ON}$) and the one corresponding to the US$_{OFF}$ intervals (MFR$_{OFF}$). The values for such a ratio range from 1.2 to 5.5 were always higher than unity anyway, hence indicating reasonably reproducible stimulus-induced activity superimposed on the spontaneous activity.
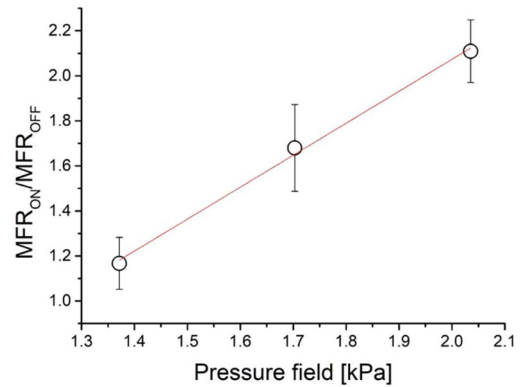
We also tested the effect of different US pulse intensities and durations on the neuronal network response. The power of the US source, expressed in W cm^{-2}, was converted into pressure field intensity as measured by a calibrated hydrophone positioned in a dummy MEA chamber where cells are seeded (figure 1(f)). Figure 6 shows an approximately linear relation between the MFR$_{ON}$/MFR$_{OFF}$ ratio, calculated for subsequent stimulation phases on the same MEA, and the generated pressure field intensity (circles). In particular, it can be deduced that below 1.1 kPa (corresponding to a power level of 0.5 W cm^{-2}) no significative response is generated (MFR$_{ON}$/MFR$_{OFF}$ ratio = 1.03).

To investigate the dependence of the modulated activity on the US pulse duration, and more generally its dynamics, we analyzed what is usually referred to as a post-stimulus time histogram (PSTH). Specifically, we computed the time distribution of the total number of spikes detected by all active electrodes in the array over 50 ms time bins (cumulative firing rate) starting from the beginning of the US pulse within the 2 s period, and averaged it for the 90 repeated pulses in the stimulation phase. Such a distribution is not uniform during US$_{ON}$ duration, yet it shows a peak ~0.3 s after the onset of the pulse (figure 7(a)). Interestingly, this feature is conserved when we apply pulses with shorter (0.5 s, figure 7(b)) and longer (1.5 s, figure 7(c)) durations to the same neuronal network. The reproducibility of such a 'pattern' in the neuronal network response dynamics becomes evident when calculating the time distribution of the cumulative firing rate for all experiments performed on the ten different neuronal cultures considered in figure 5. The average PSTH, reported in figure 7(d), clearly shows a peak in the response at around 300 ms delay from the onset of the US.

One may wonder whether the observed firing activity is simply due to the collection of independent single neuron responses or to a collective network response modulated by the US stimulation mediated by the BTNPs. In order to provide a possible answer, we applied a synaptic receptor antagonist cocktail to our neuronal culture, incubated with piezoelectric BTNPs [43, 44], acting on the main excitatory
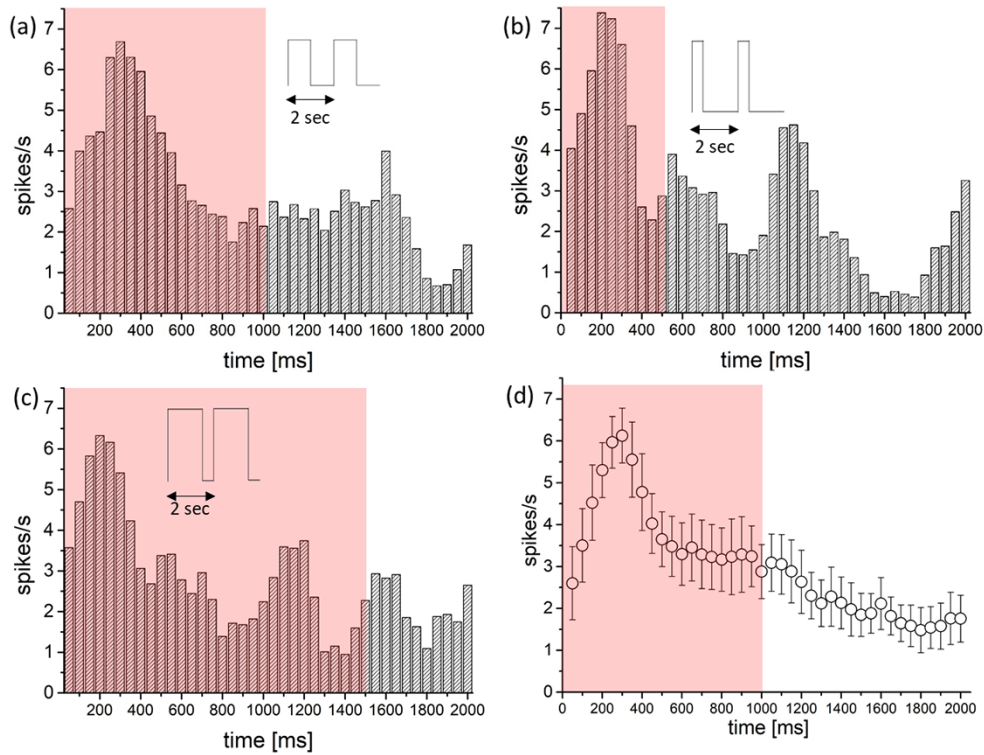
Figure 7. Time histograms of the cumulative firing rate distribution over the 2 s period during the stimulation stage (bin = 50 ms). The colored areas correspond to the duration of the US pulse: (a) 1, (b) 0.5 and (c) 1.5 s, respectively. (d) The cumulative firing rate averaged over ten experiments taken with ten different cultures (mean value and SE).
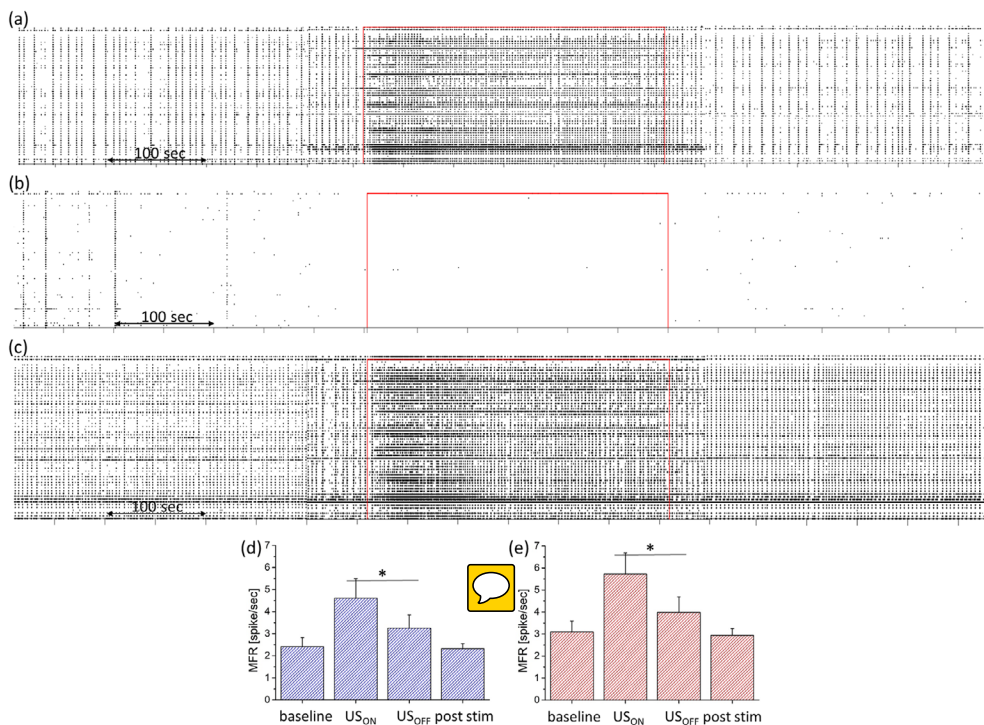

Figure 8. The network response to US stimulation modulated by synaptic blockers (BIC μ20 M APV 50 μM e CNQX 30 μM). (a)–(c) Raster plots of the activity before, during the 5 min stimulation stage (red boxes), and after it, respectively; (a) before, (b) after the addition of the synapse antagonist cocktail, and (c) after the washing out of the cocktail and 2 h in the incubator. (d) and (e) The mean network firing rate (MFR) calculated over 150 s intervals before, during and after US stimulation from the data plotted in (a) and (c), respectively ($^*P < 0.05$, Wilcoxon signed rank test).

and inhibitory receptors (GABA, AMPA and NMDA) (composition described in the methods), with the objective of isolating neurons from a network context. We monitored the electrophysiological response to US stimulation before, during and after washout of the cocktails. The Raster plots (figures 8(a)–(c)) and the computed MFR values (figure 8(d)) show that treatment with the blockers of the synaptic transmission significantly decreased the responses to piezoelectric stimulation. Ten minutes after the addition of the cocktail, as expected the spontaneous activity was drastically reduced and the US stimulation was not able to elicit any activity modulation (figure 8(b)). At this stage, the network did not show any response to electrical stimulation either (data not shown). This effect can be reversed by washing out the inhibitory cocktail with a fresh culture medium and putting the culture back into the incubator. After 2 h, both the spontaneous activity and the response to US stimulation had fully recovered, as can be appreciated from the Raster plot (figure 8(c)) and the MFR during stimulation (figure 8(e)).

For completeness, we also calculated the standard parameters to evaluate the network activity characteristics (i.e. the MFR, the mean bursting rate (MBR), the burst duration (BD) and the average inter-burst interval (IBI)) of the neuronal networks before the application of the US stimulation protocol (supporting table S1). Moreover, the inter-burst interval (IBI) distribution before, during and after stimulation (supporting figure S5) shows that US stimulation reduces the interval between bursts inducing locking around the time-period of stimulation (i.e. 2 s in our stimulation protocol), thus suggesting that US stimulation is capable of eliciting a burst response at the network level. Finally, in the same experiments, the inter-spike interval (ISI) distributions before, during and after US stimulation were evaluated and no differences were observed (supporting figure S6). Even the ISI distribution during US_{ON} and US_{OFF} intervals shows the same peak at ~3 ms, thus indicating that US stimulation greatly increases the number of spikes, but their timing is a characteristic of the network which is not affected by US.

Discussion and conclusion

After 21 d, *in vitro* neuronal cultures present spontaneous electrophysiological activity constituted by a mixture of spiking and bursting activity, including synchronized network events (i.e. network bursts). We showed that such activity can be modulated (i.e. enhanced) when US stimulation, provided as a pulse train at 1 MHz with 2 s periodicity, a variable duty cycle and amplitude, is coupled with piezoelectric nanoparticles, which we assume are adsorbed on the plasma membrane.

The spontaneous activity of different networks coming from the same cell preparation, from different animals, or from different districts of the central nervous system (cortex and hippocampus) can vary a lot in terms of network activity (MFR), network dynamics (e.g. the presence of bursting activity, synchronous oscillations), structural and functional connectivity, and, as a consequence, response to external stimulation [45]. Despite such variability we consistently observed an evident increase in the network firing rate due to US stimulation, which fully recovers to the baseline once the US is switched off (figure 5). Out of thirteen neuronal preparations, the only three that did not show any detectable response to US did not respond to electrical stimulation either.

The clear reversibility of the US-induced response allowed us to perform repeated experiments on the same cell culture, varying single parameters of US stimulation, such as intensity or pulse duration (duty cycle). In partial agreement with what was previously observed by Marino *et al* [36], who evaluated calcium flow transients, we obtained a clear dependence and a linear relationship between the relative increase in the MFR of the network and the pressure field intensity, thus suggesting that possible steering of the network activity can be implemented by fine-tuning the US amplitude. Furthermore, as reported in figure 7(d), the mean firing response to US stimulation for all tested samples shows a robust peak 200–300 ms after the US onset, and this is conserved regardless of the duration of the pulse in the 0.5–1.5 s range (figures 7(a) and (c)). After this peak, the network activity decreases to a non-excited state. This can be interpreted in terms of the time necessary to recover after network-wide activity (i.e. activity involving most of the neurons within the network) to let the synaptic machinery (e.g. supplies of synaptic vesicles) support the neuronal communication by neurotransmitter release again [46].

Our results provide further indications of the mechanism at the basis of the observed response to US stimulation. As already proposed by Marino *et al* [36], mechano(acoustic)-electric transduction seems to be a key element, but without piezoelectric properties, since we never observed an induced response in the presence of analogous nanoparticles (figure 6). Interestingly, we also observed in a preliminary experiment (figure 8) that we could 'turn off' the evoked electrical response by reversibly blocking the synaptic transmission of the network. We interpret this as an indication that even if the mechano-electric transduction performed by the piezoelectric BTNPs works at the subcellular level, the measureable effect is at the network level. Possible speculation about the related mechanism capable of enhancing network activity relies on the possibility that the locally generated electric fields (given by the BTNPs upon US stimulation) locally induce voltage membrane fluctuations, thus increasing the firing probability of already excited neurons (by the natural activation of synaptic inputs). In this case too, a systematic dissection of the glutamatergic and GABAergic components, with the antagonist of the excitatory and inhibitory synapses, together with additional experiments aimed at controlling the level of overall network excitability, would allow a better understanding of the (sub)-cellular mechanisms at the basis of the obtained network response.

To our knowledge, this is the first report on the efficient and tunable modulation of the electrophysiological activity on actual neuronal networks by means of non-invasive US stimulation mediated by piezoelectric nanoparticles. The acoustic-electric stimulation enabled by piezo-nanomaterials, without genetic intervention (as is the case for the recently proposed sonogenetic technique [47]), makes the proposed

AQ10

strategy particularly promising in terms of the possibility of generating physiologically relevant responses in a minimally invasive way. When targeting *in vivo* applications, we foresee the possibility of highly selective and efficient neural stimulation, by providing suitable nanoparticle functionalization to address specific groups of neurons in the central nervous system with virtually single cell resolution, together with the use of focused US. This represents a valuable innovative tool for the generation of new non-invasive neural interfaces, as recently discussed by Rivnay *et al* [23], thus enabling new applications in translational nanomedicine.

ORCID iDs

Gianni Ciofani ⬤ https://orcid.org/0000-0003-1192-3647
Roberto Raiteri ⬤ https://orcid.org/0000-0002-1907-7855

References

[1] ~~Dempsey C *et al* 2013 Coating barium titanate nanoparticles with polyethylenimine improves cellular uptake and allows for coupled imaging and gene delivery *Colloids Surf.* B **112** 108–12~~

[2] Fox M D *et al* 2014 Resting-state networks link invasive and noninvasive brain stimulation across diverse psychiatric and neurological diseases *Proc. Natl Acad. Sci. USA* **111** E4367–75

[3] Limousin P *et al* 1998 Electrical stimulation of the subthalamic nucleus in advanced Parkinson's disease *New Engl. J. Med.* **339** 1105–11

[4] Mazzone P, Garcia-Rill E and Scarnati E 2016 Progress in deep brain stimulation of the pedunculopontine nucleus and other structures: implications for motor and non-motor disorders *J. Neural transm.* **123** 653

[5] Bronstein J M *et al* 2011 Deep brain stimulation for Parkinson disease: an expert consensus and review of key issues *Arch. Neurol.* **68** 165

[6] Marin C and Fernández E 2010 Biocompatibility of intracortical microelectrodes: current status and future prospects *Frontiers Neuroeng.* **3** 8

[7] George M S and Aston-Jones G 2010 Noninvasive techniques for probing neurocircuitry and treating illness: vagus nerve stimulation (VNS), transcranial magnetic stimulation (TMS) and transcranial direct current stimulation (tDCS) *Neuropsychopharmacology* **35** 301–16

[8] Thielscher A, Opitz A and Windhoff M 2011 Impact of the gyral geometry on the electric field induced by transcranial magnetic stimulation *Neuroimage* **54** 234–43

[9] Thielscher A and Kammer T 2004 Electric field properties of two commercial figure 8 coils in TMS: calculation of focality and efficiency *Clin. Neurophysiol.* **115** 1697–708

[10] ~~Parasuraman R, Christensen J and Grafton S 2012 *Neuroergonomics: the Brain in Action and at Work* (New York: Academic)~~

[11] Naor O, Krupa S and Shoham S 2016 Ultrasonic neuromodulation *J. Neural Eng.* **13** 031003

[12] White P, Clement G and Hynynen K 2006 Local frequency dependence in transcranial ultrasound transmission *Phys. Med. Biol.* **51** 2293

[13] Hayner M and Hynynen K 2001 Numerical analysis of ultrasonic transmission and absorption of oblique plane waves through the human skull *J. Acoust. Soc. Am.* **110** 3319–30

[14] Tsui P H, Wang S H and Huang C C 2005 *In vitro* effects of ultrasound with different energies on the conduction properties of neural tissue *Ultrasonics* **43** 560–5

[15] Ter Haar G 2007 Therapeutic applications of ultrasound *Prog. Biophys. Mol. Biol.* **93** 111–29

[16] Krasovitski B *et al* 2011 Intramembrane cavitation as a unifying mechanism for ultrasound-induced bioeffects *Proc. Natl Acad. Sci. USA* **108** 3258–63

[17] Kubanek J, Shi J, Marsh J, Chen D, Deng C and Cui J 2016 Ultrasound modulates ion channel currents *Sci. Rep.* **6** 24170

[18] Tyler W J, Tufail Y, Finsterwald M, Tauchmann M L, Olson E J and Majestic C 2008 Remote excitation of neuronal circuits using low-intensity, low-frequency ultrasound *PLoS One* **3** 3511

[19] Tufail Y, Matyushov A, Baldwin N, Tauchmann M L, Georges J, Yoshihiro A, Helms Tillery S I and Tyler W J 2010 Transcranial pulsed ultrasound stimulates intact brain circuits *Neuron* **10** 681–94

[20] Tufail Y *et al* 2011 Ultrasonic neuromodulation by brain stimulation with transcranial ultrasound *Nat. Protocols* **6** 1453–70

[21] Yoo S-S *et al* 2011 Focused ultrasound modulates region-specific brain activity *Neuroimage* **56** 1267–75

[22] Wang Y and Guo L 2016 Nanomaterial-enabled neural stimulation *Frontiers Neurosci.* **10** 69

[23] Rivnay J *et al* 2017 Next-generation probes, particles, and proteins for neural interfacing *Sci. Adv.* **3** e1601649

[24] Pappas T C *et al* 2007 Nanoscale engineering of a cellular interface with semiconductor nanoparticle films for photoelectric stimulation of neurons *Nano Lett.* **7** 513–9

[25] ~~Molokanova E, Bartel J A, Zhao W, Naasani I, Ignatius M J, Treadway J A and Savtchenko A 2008 Quantum dots move beyond fluorescence imaging the unique properties of quantum dots allow them to be optimized for voltage sensing and for light-controlled electrical activation of cell *Biophotonics Int.* **15** 26~~

[26] Marino A *et al* 2017 Gold nanoshell-mediated remote myotube activation *ACS Nano* **11** 2494–508

[27] Nam G *et al* 2014 Facile synthesis and enhanced ultraviolet emission of ZnO nanorods prepared by vapor-confined face-to-face annealing *ACS Appl. Mater. Interfaces* **7** 873–9

[28] Fiebig M 2005 Revival of the magnetoelectric effect *J. Phys. D: Appl. Phys.* **38** R123

[29] Laurent S *et al* 2008 Magnetic iron oxide nanoparticles: synthesis, stabilization, vectorization, physicochemical characterizations, and biological applications *Chem. Rev.* **108** 2064–110

[30] Huang H *et al* 2010 Remote control of ion channels and neurons through magnetic-field heating of nanoparticles *Nat. Nanotechnol.* **5** 602–6

[31] Chen R *et al* 2015 Wireless magnetothermal deep brain stimulation *Science* **347** 1477–80

[32] Tay A and Di Carlo D 2017 Magnetic nanoparticle-based mechanical stimulation for restoration of mechano-sensitive ion channel equilibrium in neural networks *Nano Lett.* **17** 886–92

[33] Tay A *et al* 2016 Induction of calcium influx in cortical neural networks by nanomagnetic forces *ACS Nano* **10** 2331–41

[34] Wang Z L and Song J 2006 Piezoelectric nanogenerators based on zinc oxide nanowire arrays *Science* **312** 242–6

[35] Wang X *et al* 2007 Direct-current nanogenerator driven by ultrasonic waves *Science* **316** 102–5

[36] Marino A *et al* 2015 Piezoelectric nanoparticle-assisted wireless neuronal stimulation *ACS Nano* **9** 7678–89

[37] Chiappalone M *et al* 2006 Dissociated cortical networks show spontaneously correlated activity patterns during *in vitro* development *Brain Res.* **1093** 41–53

[38] Chiappalone M, Massobrio P and Martinoia S 2008 Network plasticity in cortical assemblies *Eur. J. Neurosci.* **28** 221–37

[39] Bologna L L *et al* 2010 Investigating neuronal activity by SPYCODE multi-channel data analyzer *Neural Netw.* **23** 685–97

[40] Maccione A *et al* 2009 A novel algorithm for precise identification of spikes in extracellularly recorded neuronal signals *J. Neurosci. Methods* **177** 241–9

[41] Rolston J D, Wagenaar D A and Potter S M 2007 Precisely timed spatiotemporal patterns of neural activity in dissociated cortical cultures *Neuroscience* **148** 294–303

[42] Wagenaar D A, Pine J and Potter S M 2006 An extremely rich repertoire of bursting patterns during the development of cortical cultures *BMC Neurosci.* **7** 11

[43] Gal A *et al* 2010 Dynamics of excitability over extended timescales in cultured cortical neurons *J. Neurosci.* **30** 16332–42

[44] Kanagasabapathi T T *et al* 2013 Selective pharmacological manipulation of cortical–thalamic co-cultures in a dual-compartment device *J. Neurosci. Methods* **214** 1–8

[45] Massobrio P, Pasquale V and Martinoia S 2015 Self-organized criticality in cortical assemblies occurs in concurrent scale-free and small-world networks *Sci. Rep.* **5**

[46] Cohen D and Segal M 2011 Network bursts in hippocampal microcultures are terminated by exhaustion of vesicle pools *J. Neurophysiol.* **106** 2314–21

[47] Ibsen S *et al* 2015 Sonogenetics is a non-invasive approach to activating neurons in Caenorhabditis elegans *Nat. Commun.* **6**